Supplementary Information

Stability of Organic Ligands on the Oxygen Evolving Center of Photosystem II and Manganese Oxide Water Oxidation Catalysts

Toru Hayashi[a], Akira Yamaguchi[b], Kazuhito Hashimoto[c], and Ryuhei Nakamura[b]

(a) Department of Applied Chemistry, The University of Tokyo,
7-3-1 Hongo, Bunkyo-ku, Tokyo 113-8656, Japan.
(b) Biofunctional Catalyst Research Team, RIKEN Center for Sustainable Resource Science (CSRS), 2-1 Hirosawa, Wako, Saitama 351-0198, Japan.
(c) National Institute for Materials Science (NIMS),
1-2-1 Sengen, Tsukuba, Ibaraki 305-0047, Japan.

Contents

Synthesis of α-MnO_2 Powder

α-MnO_2 powder was synthesized as previously reported [S1,S2]. 1.10 g of $KMnO_4$ in 20 ml of water was stirred for 30 min at 60 °C. Separately, 1.89 g of $MnSO_4 \cdot 5H_2O$ in 25 ml of a 2 M acetic acid aqueous solution was stirred for 20 min at room temperature. The solutions were mixed and heated for 2 h at 80 °C under a stirred condition. The particles thus obtained were collected, washed, and dried overnight at 60 °C.

Preparation of α-MnO_2 Particulate Film Electrodes

Particulate film electrodes of α-MnO_2 were prepared by a spray deposition method as previously described [S3]. The amount of deposited α-MnO_2 was ~0.14 mg cm^{-2} unless otherwise noted. In this case, 75 mg of the α-MnO_2 powder was ground in an agate mortar for 5 min, and suspended in 100 mL of highly pure Milli-Q water (18 MΩ cm^{-1}) by a sonicator (Q700, QSonica). The suspension was sprayed by a spray gun (ST-6, Fuso Seiki Co., Ltd.) onto a clean conducting fluorine-tin-oxide-coated glass substrate (SPD Laboratory, Inc.) heated at 200 °C. The electrodes were gently washed with the highly pure Milli-Q water, and calcined in air for 4 h at 500 °C. The deposited amount was controlled by the initial amount of the α-MnO_2 powder.

Details of Measurement Method

Electrochemical Measurement in General

Current density (j) and potential (U) were controlled and measured with a commercial potentiostat and potential programmer (HZ-5000, Hokuto Denko), using a Pt wire as the counter electrode and a Ag/AgCl/KCl (saturated) electrode as the reference electrode. Sodium sulfate was used as the supporting electrolyte with the concentration set at 0.5 M. Sodium benzoate, imidazole, and guanidine sulfate were used as artificial amino-acid analogs and were introduced by dissolving them into the electrolyte. The electrolyte solution was prepared using the highly pure Milli-Q water and reagent-grade chemicals, and the pH was adjusted using 1.0 M H_2SO_4 and 1.0 M NaOH. Guanidine sulfate and isotopic reagents (D_2O, and D_2SO_4 for pD adjustment) were obtained from Sigma-Aldrich, and all other reagents are obtained from Wako and used without further purification.

O_2 Measurement by a Fluorescence-Based Needle-Type O_2 Microsensor (OMS)

The concentration of dissolved O_2 in the electrolyte solution was monitored using a fluorescence-based needle-type OMS (Microx TX3-trace, PreSens) under stirred condition.

Tafel Plots

Tafel plots were made by plotting steady-state current at each potential. The electrolyte was filled and stirred by a stir bar at *ca.* 1000 rpm. The amount of deposited α-MnO_2 was decreased to be ~0.056 mg cm^{-2} to lessen the effect of pseudo-capacitance. The highest potential was kept for more than 500 s to avoid the effect of pseudo-capacitance. At other potentials, the steady-state current was measured after 90 s. The solution resistance was measured and the resulting ohmic potential loss was corrected.

pH Dependence of Potential under a Constant Current Condition

pH dependence of potential under a constant current condition was measured by plotting the potential during the change of pH by the addition of NaOH aq. The electrolyte was filled and stirred by a stir bar at *ca.* 800 rpm. The amount of deposited α-MnO_2 was decreased to be ~0.056 mg cm^{-2} to lessen the effect of pseudo-capacitance. Although ohmic potential loss cannot be corrected because of the change in the composition of the electrolyte, the change in the solution resistance was so small that the slope value was not affected in the experimental accuracy in this time.

Kinetic Isotope Effect (KIE) Measurement

KIE was measured based on the ratio of current density during linear sweep voltammetry. The concentration of sodium benzoate was 0.5 M, and the scan rate was 10 mV s^{-1}. pD was adjusted based on the relationship between pD and pH: pD = pH + 0.4 [S4]. The amount of deposited α-MnO_2 was ~0.056 mg cm^{-2}. The KIE was calculated at the potentials where the current density reaches 0.25 mA cm^{-2} in undeuterated electrolyte. The measurement was conducted twice.

FT-IR spectroscopy

The structure of bases on the surface of α-MnO_2 was analyzed by a Fourier transform infrared (FT-IR) spectrometer (Vertex 70, Bruker). 60 mg of α-MnO_2 powder was immersed in 10 mL of the solution of sodium benzoate or imidazole with 0.1 M deprotonated anions whose pH was adjusted to 7.5 by H_2SO_4 or NaOH. The solution was stirred for 12 h. The powder was then separated by suction filtration with a hydrophilic PTFE membrane filter with a 0.2 μm pore size (JGWP04700, Merck Millipore), followed by vacuum drying in a Schlenk flask. As a control sample, α-MnO_2 powder immersed in the highly pure Milli-Q water was also prepared. After ground in an agate mortar, 20 mg of the dried powder was pressed by a hydraulic press (SSP-10A, Shimadzu) into a pellet with a diameter of 12 mm for the measurement.

Inlet Electrochemical Mass Spectroscopy (EC-MS)

EC-MS was also performed to measure the onset potentials of O_2 and CO_2 evolution. The principle of the EC-MS system was the same as previously reported [S5,S6]. A stainless capillary connected a gas-tight electrochemical chamber and a quadrupole mass spectrometer (QMG 220 M1, Pfeiffer Vacuum). The end of the capillary in the electrochemical chamber was covered with a microporous polytetrafluoroethylene (PTFE) membrane (Poreflon WP-010-80, Sumitomo Electric Fine Polymer). Before measuring the evolution of O_2 or CO_2, the electrochemical chambers were bubbled with argon for 30 minutes.

In-situ UV-vis Spectroscopy

Optical absorption of electrodes in contact with the electrolyte was measured by a UV-vis spectrometer (UV-2550, Shimadzu) equipped with a multipurpose large-sample compartment with a built-in integrating sphere (MPC-2200, Shimadzu), by placing electrodes in front of the integrating sphere and collecting diffused transmission light. The amount of deposited α-MnO_2 was decreased to be ~0.056 mg cm^{-2} to lessen the original absorption by the catalyst.

Supplementary Figures and Table

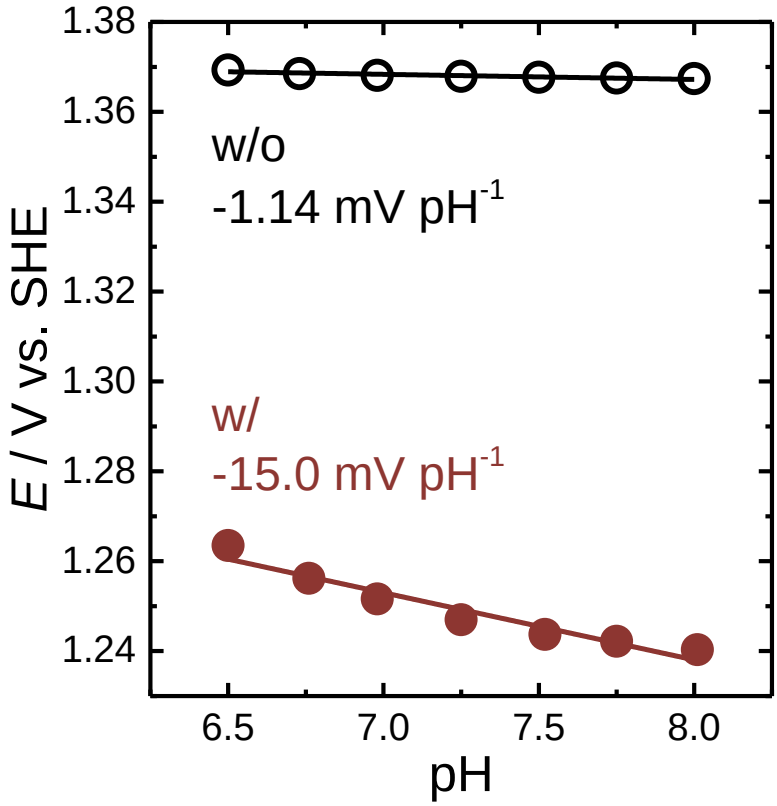

Fig. S1 pH dependence of potential at a constant current density (50 μA cm^{-2}) in the absence and presence of 50 mM of benzoate.

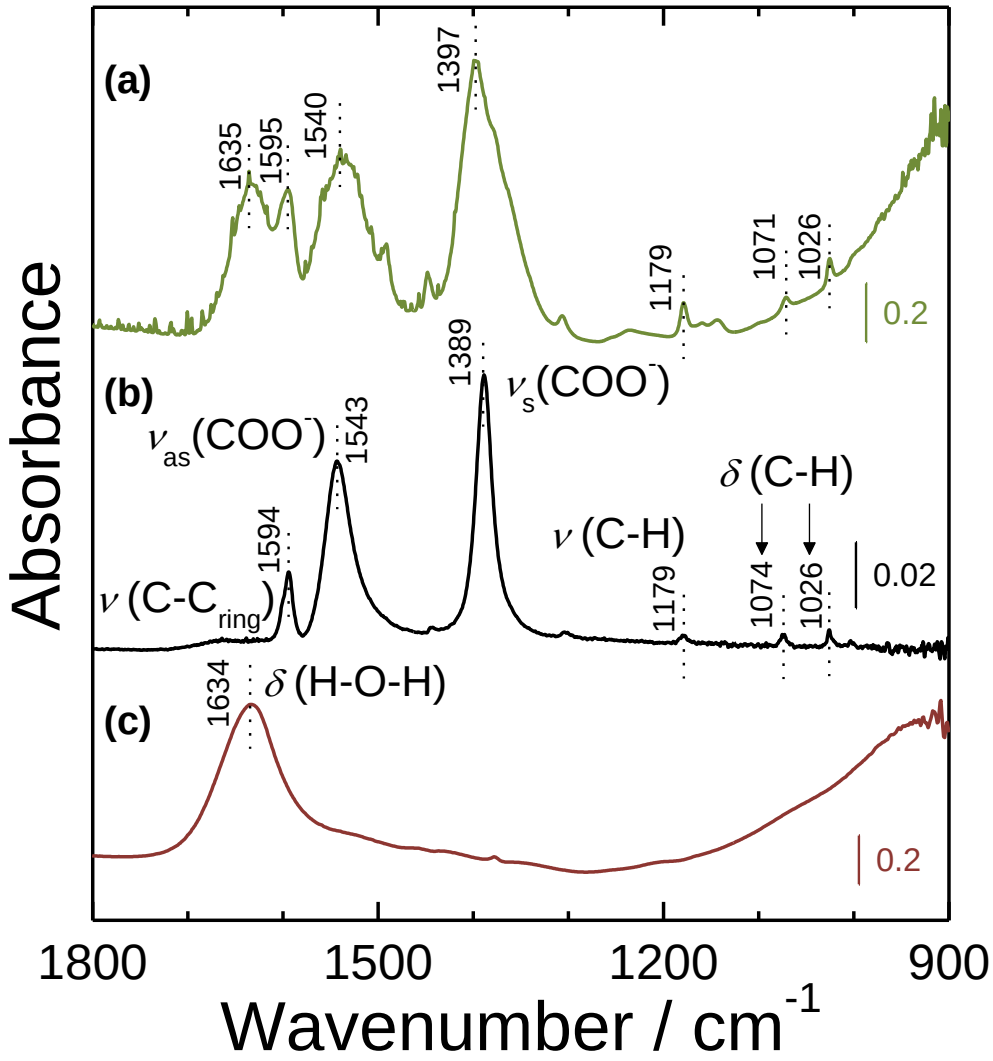

Fig. S2 FT-IR spectra of (a) α-MnO_2 after the immersion in the solution of 0.1 M deprotonated benzoate at pH 7.5 adjusted by NaOH for 12 h, (b) the solution of 0.1 M deprotonated benzoate at pH 7.5 adjusted by NaOH, and (c) α-MnO_2. In (b), the observed peaks at 1388 cm^{-1} and 1541 cm^{-1} can be assigned to the symmetric and asymmetric stretching mode of COO^- ($\nu_s(COO^-)$ and $\nu_{as}(COO^-)$), respectively [S7,S8]. The peak at 1594 cm^{-1} can be assigned to the stretching mode of C-C (aromatic ring) (ν(C-C_{ring})) [S7,S8]. The small peak at 1179 cm^{-1} was assigned to a C-H stretching mode, and those at 1071 cm^{-1} and 1026 cm^{-1} were assigned to C-H in-plane bending modes [S9]. In (a), the band of $\nu_s(COO^-)$ shifted to higher frequency region, which indicated the chemisorption of benzoate on the surface of α-MnO_2 [S7]. The small shift (8 cm^{-1}), as well as broadening of the bands of $\nu_s(COO^-)$ and $\nu_{as}(COO^-)$, is in favor of the formation of outer-sphere complexes [S7]. On the other hand, the positions of the bands from the aromatic ring was almost constant. Those results indicate that benzoate formed outer-sphere complexes with the surfaces of α-MnO_2, as shown in Fig. S3, which is a suitable conformation for the induction of CPET.

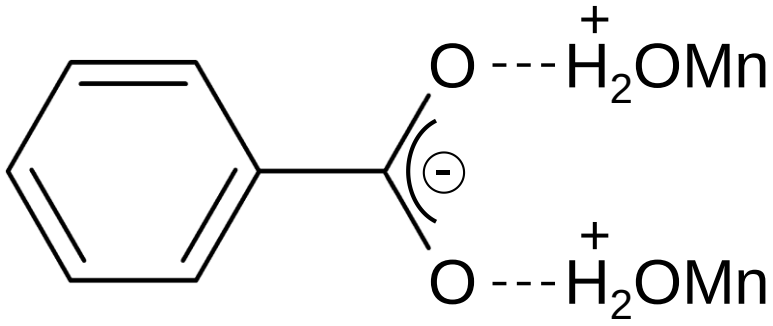

Fig. S3 Schematic representation of surface complexation of benzoate on the surface of α-MnO_2 [S7].

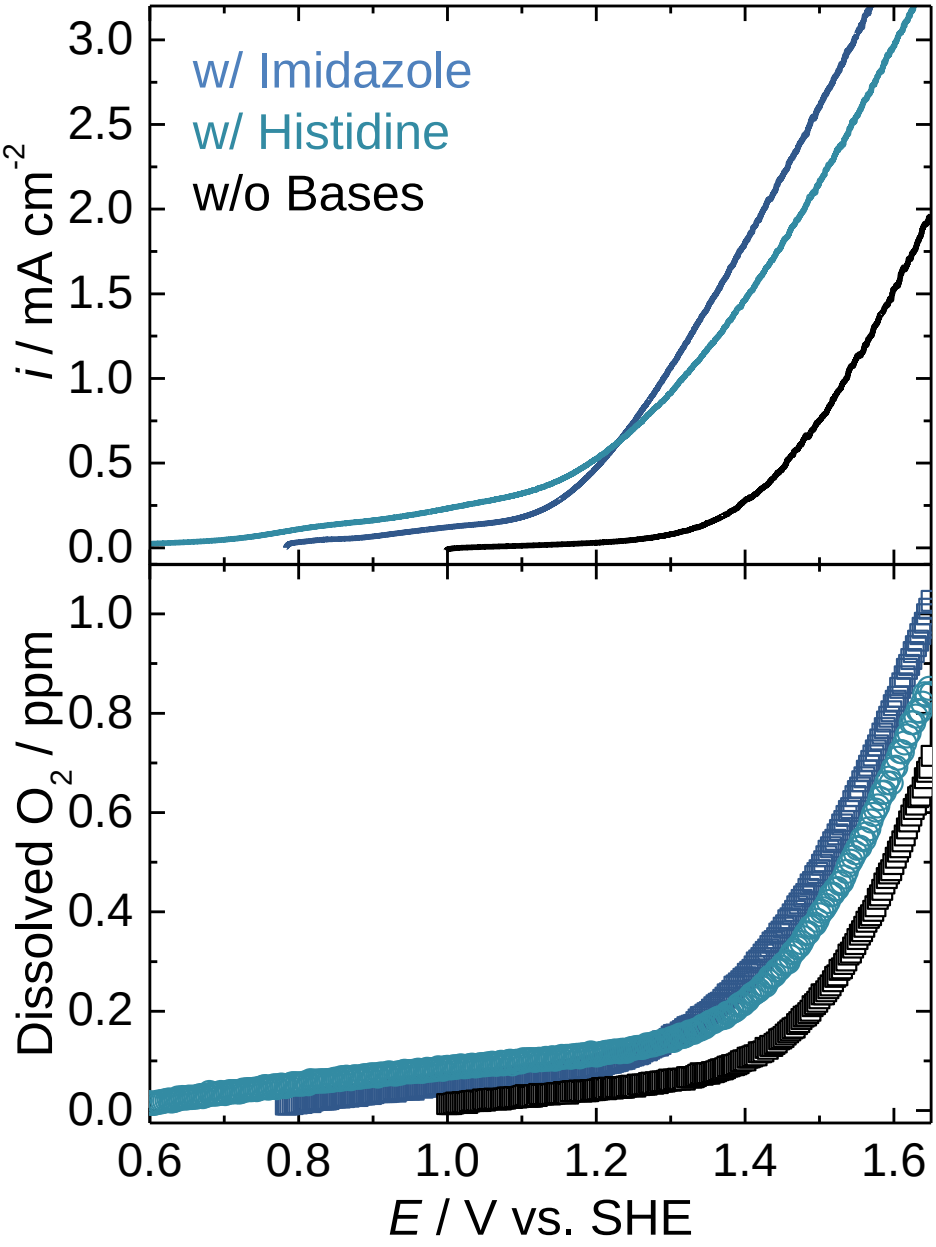

Fig. S4 Potential dependence of current density and dissolved amount of O_2 in the presence of imidazole or histidine (pH 7.5, Scan rate: 1 mV s^{-1}, Concentration of deprotonated imidazole ring: 50 mM).

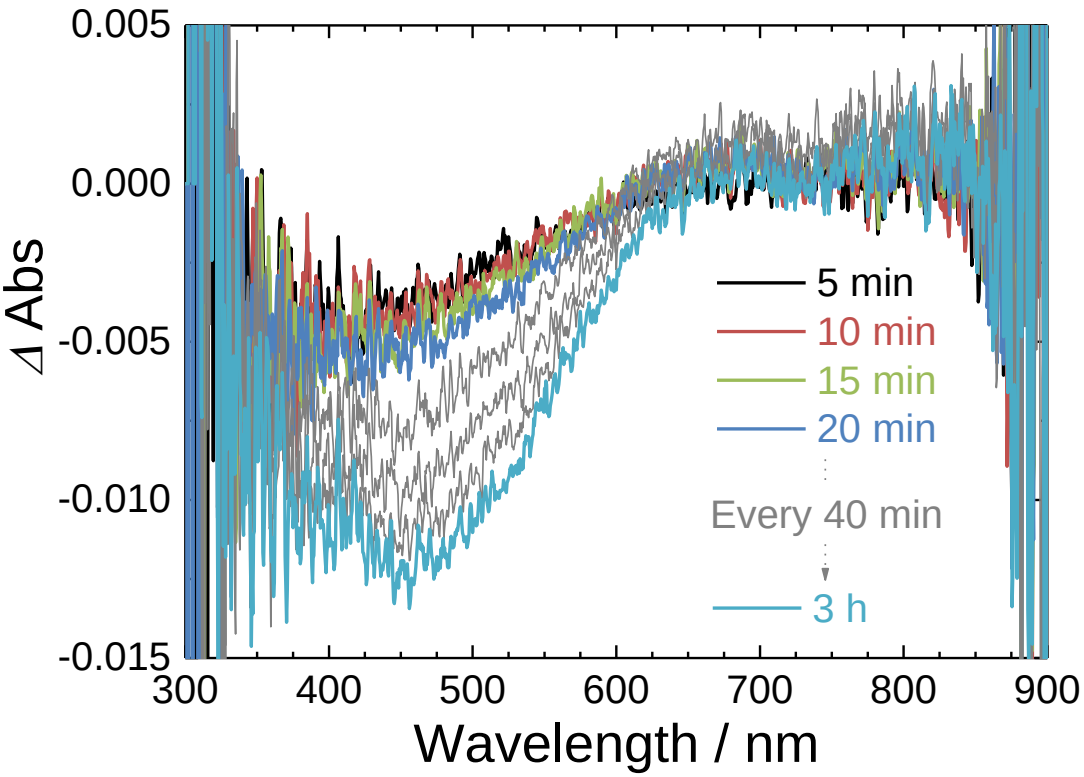

Fig. S5 Changes in the UV-Vis spectra of an α-MnO_2 electrode in contact with the electrolyte which contained 500 mM deprotonated imidazole (pH 7.5) at rest potential. The spectrum immediately after the contact with the electrolyte was used as a reference.

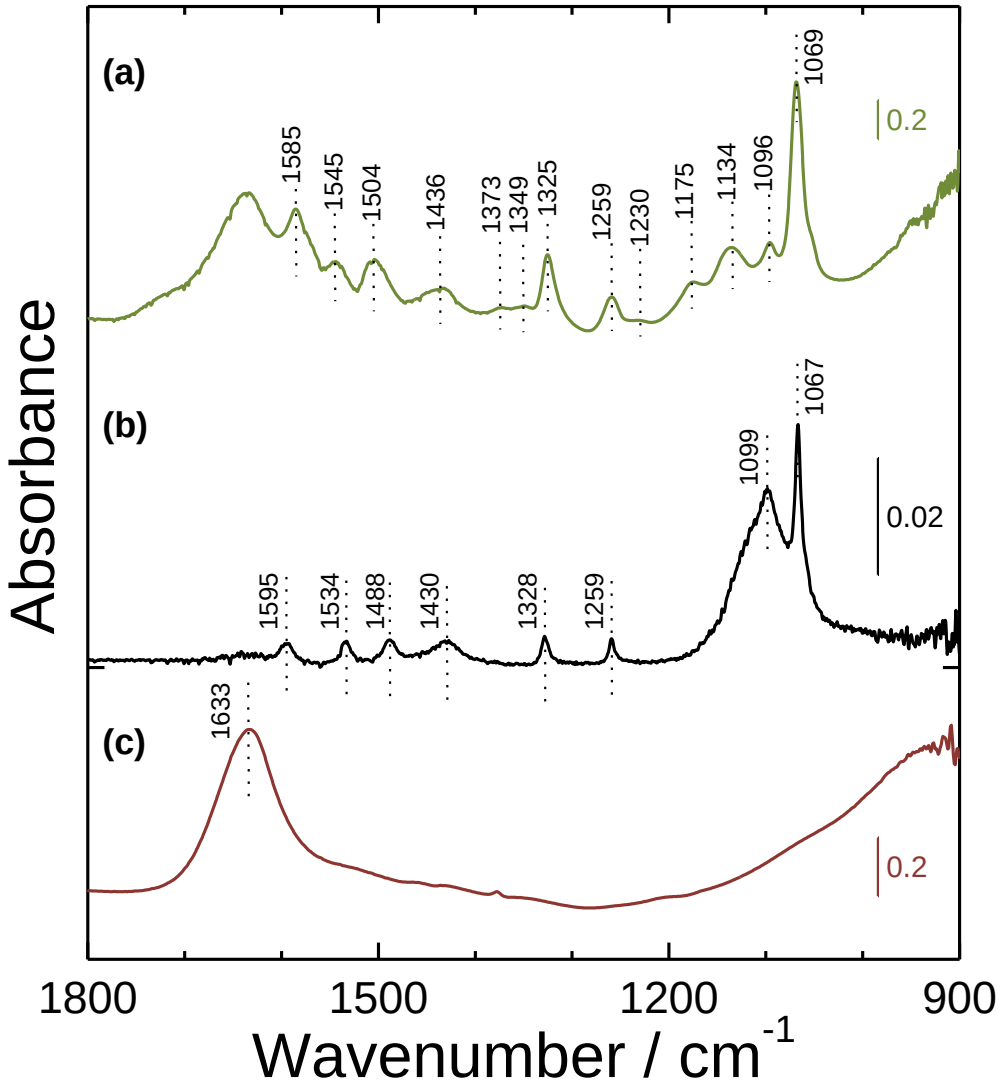

Fig. S6 FT-IR spectra of (a) α-MnO_2 after the immersion in the solution of 0.1 M deprotonated imidazole at pH 7.5 adjusted by H_2SO_4 for 12 h, (b) the solution of 0.1 M deprotonated imidazole at pH 7.5 adjusted by H_2SO_4, and (c) α-MnO_2. The number of peaks increased after the interaction with α-MnO_2, compared to the spectra of the imidazole solution. We regard the new peaks can be assigned to the oxidation products. The derivatives of urea or nitronate were shown as oxidation products of imidazolyl groups in the previous studies [S10-12], which can be the candidates of the products in our cases.

***E*$_1$ of Imidazole**

Equilibrium between Differently Protonated States of Imidazole and Imidazole Radicals

First, the equilibrium between differently protonated states of imidazole and imidazole radicals are summarized in Scheme S1.

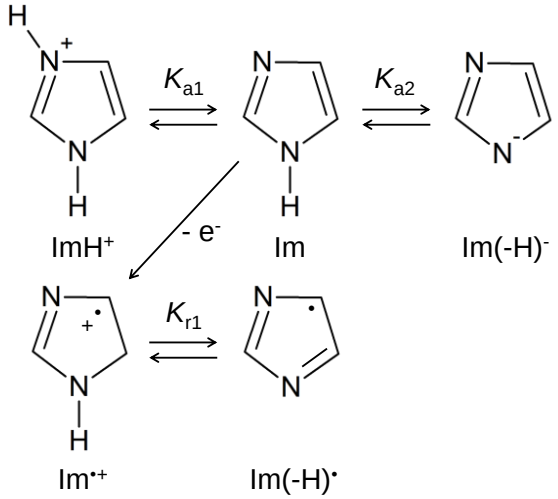

Scheme S1 Protonation equilibrium of imidazole and imidazole radicals.

ImH$^{\bullet\,2+}$, the protonated form of Im$^{\bullet\,+}$, is thermodynamically unstable and deprotonates, thus virtually does not exist. Equilibrium constants are given by following equations:

$$K_{a1} = \frac{[Im][H^+]}{[ImH^+]},\ K_{a2} = \frac{[Im(\text{-H})^-][H^+]}{[Im]},\ K_{r1} = \frac{[Im(\text{-H})^{\cdot}][H^+]}{[Im^{\cdot\,+}]}$$

pK_{a1} = 7.05 and pK_{a2} = 14.5 [S13]; pK_{r1} has not been reported to our knowledge.

Conversion of Vertical Ionization Energy (VIE) to E_1

As mentioned in the main text, experimental values of the redox potential of the one-electron oxidation (E_1) of imidazole has not been reported so far to our knowledge. However, an experimental value of the vertical ionization energy (VIE) of imidazole has been reported by a study using photoelectron spectroscopy of liquid microjet [S14]. Thus, the standard E_1 (E_1^0(Im$^{\bullet+}$/Im)) can be obtained by subtracting outer-sphere reorganization energy (λ) from VIE.

According to the report, the VIE of neutral imidazole (Im) is +3.98 V vs. SHE [S14]. Here, VIE vs. SHE was calculated by using the reported potential of SHE vs. vacuum, +4.28 V [S15, S16]. λ is estimated to be smaller than 1 eV as for the reactions on electrodes in water with the diameter of the reactant larger than 2 Å [S17]. Thus, E_1^0(Im$^{\bullet+}$/Im) can be estimated to be more positive than +2.98 V vs. SHE.

pH dependence

Analysis of the pH dependence of E_1 requires consideration of the protonation equilibrium and can be estimated by reference to the method reported by Schroeder *et al.*[S18]

Here, $[\mathrm{Im}]_{\mathrm{total}}$ and $[\mathrm{Im}^{\bullet}]_{\mathrm{total}}$ are defined as follows:

$$[\mathrm{Im}]_{\mathrm{total}} = [\mathrm{ImH}^+] + [\mathrm{Im}] + [\mathrm{Im(-H)}^-] = [\mathrm{Im}] \cdot \left(\frac{[\mathrm{H}^+]}{K_{\mathrm{a1}}} + 1 + \frac{K_{\mathrm{a2}}}{[\mathrm{H}^+]} \right)$$

$$[\mathrm{Im}^{\cdot}]_{\mathrm{total}} = [\mathrm{Im}^{\cdot +}] + [\mathrm{Im(-H)}^{\cdot}] = [\mathrm{Im}^{\cdot +}] \cdot \left(1 + \frac{K_{\mathrm{r1}}}{[\mathrm{H}^+]} \right)$$

Thus,

$$[\mathrm{Im}] = [\mathrm{Im}]_{\mathrm{total}} \cdot \frac{K_{\mathrm{a1}}[\mathrm{H}^+]}{[\mathrm{H}^+]^2 + K_{\mathrm{a1}}[\mathrm{H}^+] + K_{\mathrm{a1}}K_{\mathrm{a2}}}$$

$$[\mathrm{Im}^{\cdot +}] = [\mathrm{Im}^{\cdot}]_{\mathrm{total}} \cdot \frac{[\mathrm{H}^+]}{[\mathrm{H}^+] + K_{\mathrm{r1}}}$$

Thus, a Nernst equation for E_1 can be written as follows:

$$E_1 = E_1{}^0(\mathrm{Im}^{\cdot +}/\mathrm{Im}) + \frac{RT}{F} \ln \left(\frac{[\mathrm{Im}^{\cdot +}]}{[\mathrm{Im}]} \right) = E_1{}^0(\mathrm{Im}^{\cdot +}/\mathrm{Im}) + \frac{RT}{F} \ln \left(\frac{1}{K_{\mathrm{a1}}} \cdot \frac{[\mathrm{H}^+]^2 + K_{\mathrm{a1}}[\mathrm{H}^+] + K_{\mathrm{a1}}K_{\mathrm{a2}}}{[\mathrm{H}^+] + K_{\mathrm{r1}}} \right)$$

Note that $[\mathrm{Im}]_{\mathrm{total}}$ equals to $[\mathrm{Im}^{\bullet}]_{\mathrm{total}}$ at E_1. By substitution of the pK values, E_1 at the standard condition at pH 7.5 can be calculated as follows:

$$E_1 \text{ / V vs. SHE} = E_1{}^0(\mathrm{Im}^{\bullet +}/\mathrm{Im}) \text{ / V vs. SHE} - 0.4359 - 0.05916 \log_{10}(10^{-7.5} + K_{\mathrm{r1}})$$

Here, $E_1{}^0(\mathrm{Im}^{\bullet +}/\mathrm{Im})$ corresponds to the E_1 estimated from the VIE. Therefore, for E_1 to be more negative than E_{onset} (@ 75 μA cm^{-2}) in the presence of imidazole at pH 7.5, even when λ = 1 eV, pK_{r1} have to be less than -27.6. pK_{r1} has not been reported to our knowledge, but considering that the corresponding pK value of histidine is 5-7 [S19], we can safely estimate that pK_{r1} is larger than -27.6. Thus, E_{onset} (@ 75 μA cm^{-2}) (Fig. 4) can be estimated to be well more negative than E_1.

References

[S1] R. M. McKenzie, The synthesis of birnessite, cryptomelane, and some other oxides and hydroxides of manganese. *Mineral. Mag.*, 1971, **38**, 493-502.

[S2] M. Singh, D. N. Thanh, P. Ulbrich, N. Strnadová and F. Štěpánek, Synthesis, characterization and study of arsenate adsorption from aqueous solution by α- and δ-phase manganese dioxide nanoadsorbents. *J. Solid State Chem.*, 2010, **183**, 2979–2986.

[S3] A. Yamaguchi, R. Inuzuka, T. Takashima, T. Hayashi, K. Hashimoto and R. Nakamura, Regulating proton-coupled electron transfer for efficient water splitting by manganese oxides at neutral pH. *Nat. Commun.*, 2014, **5**, 4256.

[S4] A. K. Covington, M. Paabo, R. A. Robinson and R. G. Bates, Use of the glass electrode in deuterium oxide and the relation between the standardized pD (pa_D) scale and the operational pH in heavy water. *Anal. Chem.*, 1968, **40**, 700–706.

[S5] K. Kamiya, K. Hashimoto and S. Nakanishi, Graphene defects as active catalytic sites that are superior to platinum catalysts in electrochemical nitrate reduction. *ChemElectroChem*, 2014, **1**, 858-862.

[S6] A. H. Wonders, T. H. M. Housmans, V. Rosca and M. T. M. Koper, On-line mass spectrometry system for measurements at single-crystal electrodes in hanging meniscus configuration. *J. Appl. Electrochem.*, 2006, **36**, 1215-1221.

[S7] K. D. Dobson and A. J. McQuillan, In situ infrared spectroscopic analysis of the adsorption of aromatic carboxylic acids to TiO_2, ZrO_2, Al_2O_3, and Ta_2O_5 from aqueous solutions. *Spectrochim. Acta, Part A*, 2000, **56**, 557-565.

[S8] M. R. Das and S. Mahiuddin, Kinetics and adsorption behaviour of benzoate and phthalate at the α-alumina–water interface: Influence of functionality. *Colloids Surf., A*, 2005, **264**, 90-100.

[S9] S. Tunesi and M. A. Anderson, Surface effects in photochemistry: an in situ cylindrical internal reflection-Fourier transform infrared investigation of the effect of ring substituents on chemisorption onto titania ceramic membranes. *Langmuir*, 1992, **8**, 487-495.

[S10] K. Uchida and S. Kawakishi, Selective oxidation of imidazole ring in histidine residues by the ascorbic acid – copper ion system. *Biochem. Biophys. Res. Commun.*, 1986, **138**, 659-665.

[S11] K. Uchida and S. Kawakishi, Ascorbate-mediated specific oxidation of the imidazole ring in a histidine derivative. *Bioinorg. Chem.*, 1989, **17**, 330-343.

[S12] X. Xing, X. Zhu, H. Li, Y. Jiang and J. Ni, Electrochemical oxidation of nitrogen-heterocyclic compounds at boron-doped diamond electrode. *Chemosphere*, 2012, **86**, 368-375.

[S13] H. Walba and R. W. Isensee, Acidity constants of some arylimidazoles and their cations. *J. Org. Chem.*, 1961, **26**, 2789–2791.

[S14] B. Jagoda-Cwiklik, P. Slavíček, L. Cwiklik, D. Nolting, B. Winter and P. Jungwirth, Ionization of imidazole in the gas phase, microhydrated environments, and in aqueous solution. *J. Phys. Chem. A*, 2008, **112**, 3499-3505.

[S15] C. P. Kelly, C. J. Cramer and D. G. Truhlar, Aqueous solvation free energies of ions and ion-water clusters based on an accurate value for the absolute aqueous solvation free energy of the proton. *J. Phys. Chem. B*, 2006, **110**, 16066-16081.

[S16] A. A. Isse and A. Gennaro, Absolute potential of the standard hydrogen electrode and the problem of interconversion of potentials in different solvents. *J. Phys. Chem. B*, 2010, **114**, 7894-7899.

[S17] G. J. Kavarmos, *Fundamentals of photoinduced electron transfer*. VCH, Weinheim, New York, 1993.

[S18] C. A. Schroeder, E. Pluhařová, R. Seidel, W. P. Schroeder, M. Faubel, P. Slavíček, B.Winter, P. Jungwirth and S. E. Bradforth, Oxidation half-reaction of aqueous nucleosides and nucleotides via photoelectron spectroscopy augmented by ab initio calculations. *J. Am. Chem. Soc.*, 2015, **137**, 201-209.

[S19] S. Navaratnam and B. J. Parsons, Reduction potential of histidine free radicals: A pulse radiolysis study. *J. Chem. Soc., Faraday Trans.*, 1998, **94**, 2577-2581.